Physics – Uspekhi **61** (11) 1127 – 1136 (2018)

CONFERENCES AND SYMPOSIA

PACS numbers: **75.75. – c**, **75.76. + j**, 75.78.Cd, 75.78.Jp, 78.20.Ls

Ultrafast spin dynamics and inverse spin Hall effect in nanostructures with giant spin-orbit coupling

A K Zvezdin, M D Davydova, K A Zvezdin

DOI: https://doi.org/10.3367/UFNe.2017.12.038309

Contents

Abstract. The features of ultrafast spin dynamics excitation using high-intensity femtosecond laser pulses in magnetic materials are reviewed. Key mechanisms of a pump pulse action on the spin system of a magnetic material are discussed, including the inverse Faraday effect in yttrium-iron garnet; induced magnetic anisotropy in the thulium orthoferrite, and the thermal driving of a magnetic system out of equilibrium in the case of the metallic ferrimagnet GdFeCo, which is a promising material for magnetic memory and terahertz spintronics. It was shown that, apart from using conventional magneto-optical methods for probing the magnetization dynamics in magnetic heterostructures, the inverse spin Hall effect can also be used, an approach that potentially enables the development of memory elements in which the ultrafast optical control of magnetization is combined with electrical detection.

A K Zvezdin Prokhorov General Physics Institute, Russian Academy of Sciences, ul. Vavilova 38, 119991 Moscow, Russian Federation; Lebedev Physical Institute of the Russian Academy of Sciences, Leninskii prosp. 53, 119991 Moscow, Russian Federation; Moscow Institute of Physics and Technology (State University), Institutskii per. 9, 141701 Dolgoprudnyi, Moscow region, Russian Federation
E-mail: zvezdin@gmail.com
M D Davydova, K A Zvezdin Prokhorov General Physics Institute of the Russian Academy of Sciences, ul. Vavilova 38, 119991 Moscow, Russian Federation; Moscow Institute of Physics and Technology (State University), Institutskii per. 9, 141701 Dolgoprudnyi, Moscow region, Russian Federation
E-mail: davydova@phystech.edu, konstantin.zvezdin@gmail.com

Received 18 February 2018
Uspekhi Fizicheskikh Nauk **188** (11) 1238 – 1248 (2018)
DOI: https://doi.org/10.3367/UFNr.2017.12.038309
Translated by S N Gorin; edited by A Radzig

Keywords: ultrafast spin dynamics, inverse spin Hall effect, spin pumping, magnetic nanodots, inverse Faraday effect, photomagnetic effect, photomagnetic anisotropy, laser pulse demagnetization, critical enhancement of dynamics

1. Introduction

In the last decade, a new area — ultrafast magnetism — has emerged and undergone much development in the physics of condensed media [1]. Because of the need for ever-increasing speeds of recording information, its density, and energy efficiency, and because of the gradual exhaustion of the potential of traditional electronics, the optical control of magnetization on picosecond time scales has become an especially attractive area of studies.

It has been shown that ultrashort laser pulses of high intensity can excite spin dynamics in magnetic materials, which is of significant interest from both the fundamental and the applied viewpoints. The basic experimental procedure in this field is the pump–probe technique [2–9]. The exciting pump pulse of the electromagnetic radiation has an intensity of $10^{10} - 10^{13}$ W cm^{-2} and a duration of 10–100 fs. Then, with a fixed time delay, a measuring (probe) pulse of the same duration comes, albeit with an intensity that is several orders of magnitude less. Depending on the properties of the magnetic medium, the pump pulse leads to an ultrafast demagnetization or magnetization reversal of the sample or to the excitation of a magnetization precession. Several mechanisms owing to which the action of a pump pulse can excite the ultrafast dynamics of magnetization can be mentioned, e.g., local heating of the sample [8, 10, 11], photoinduced magnetic anisotropy [12, 13], and inverse magneto-optical effects [5–7, 14, 15] (for example, the inverse Faraday, Kerr, or Cotton–Mouton effects).

In the pioneering work of Beaurepaire et al. [11], the possibility of a sharp decrease in the nickel magnetization with the aid of ultrashort laser pulses with a duration of 60 fs

was first shown. Later on, important studies were carried out, in which the possibility was demonstrated of switching the magnetization in the amorphous GdFeCo alloy depending on circular polarization in the absence of external magnetic fields [8].

In magnetically ordered materials, the inverse Faraday effect (IFE) was first discovered with the aid of the pump–probe technique with the use of femtosecond laser pulses [2]. Pulses of laser radiation with a duration of 200 fs were focused onto a spot with a diameter of 200 μm on a sample of dysprosium orthoferrite $DyFeO_3$, and the precession of the magnetization caused by such pulses was observed. This work [2] led to great interest, and later experiments were carried out that demonstrated the excitation of the dynamics of magnetization by femtosecond laser pulses in rare-earth iron garnets [4–6, 12] and in the paramagnetic crystals of dysprosium aluminum garnet $Dy_3Al_5O_{12}$ [7] and terbium–gallium garnet $Tb_3Ga_5O_{12}$ [6].

Let us consider two characteristic examples of the realization of this approach for the excitation and investigation of the dynamics of magnetization in magnetic dielectrics: in iron–yttrium garnet $R_3Fe_5O_{12}$ (R is a rare-earth element) and in orthoferrites $RFeO_3$. In the first case, an optical pulse with wavelength $\lambda = 650$ nm was used for the excitation of the magnetization dynamics, and in the second case, a terahertz laser pulse was put in operation. Another example concerns research on the excitation and dynamics of magnetization in metallic magnets, among which the ferrimagnet GdFeCo occupies a special position from both the fundamental and practical points of view [8, 6–19]. The mechanism of the excitation of coherent spin dynamics in metallic magnets differs from that in dielectrics and consists of local demagnetization, as a result of which the magnetic system moves out of equilibrium and the magnetization precession begins.

Another interesting approach to the measurement of the dynamics of magnetization induced by ultrashort laser pulses, besides the magneto-optical one, is the employment of spin-to-charge conversion, for example, based on the inverse spin Hall effect (ISHE), which will be discussed in detail in Section 5. This effect, like other spin-orbit effects, constitutes the basis for a novel branch of spintronics — spin-orbitronics [20, 21]. The motivation for these studies is the development of memory elements based on the ultrafast optical switching of magnetization in combination with electrical detection, which can be realized in the spin-orbitronics devices. In particular, spintronic terahertz emitters are actively being developed today, which are based on the inverse spin Hall effect (see review [22] and references cited therein). The operation of such devices is based on the excitation of magnetization in a ferromagnetic layer with the aid of a femtosecond laser pulse. Because of the effect of spin pumping, spin currents are generated in the system, which, because of the inverse spin Hall effect, are converted into strong nonequilibrium charge currents, which come out as antennas generating emission in the terahertz range.

If ultrafast control of spin dynamics is achieved on the nanoscale, it can be utilized in the future to resolve the problem of the creation of nano-sized energy-efficient magnetic memory cells and computational elements. In particular, plasmon nanostructures [1], in which fields may be successfully concentrated on a sub-wavelength scale, can become a key to the miniaturization of the switching area.

2. Dynamics of magnetization under the action of a femtosecond laser pulse in iron-garnet films. Inverse Faraday effect

The authors of Ref. [23] have investigated, using pump pulses with wavelength $\lambda = 650$ nm, the ultrafast dynamics of magnetization in iron-garnet films. Since the frequency of the pump pulses lay in the range of the transparency of the material, the magnetization dynamics was associated with the inverse Faraday effect (IFE) in the iron garnet; in this case, a nonlinear dependence of the IFE magnitude on the intensity of the pulse of optical pumping was discovered. Let us describe the IFE in terms of the effective magnetic field H_F of the lased pulse in the medium [2]:

$$\mathbf{H}_F = -\mathrm{i}a\frac{\varepsilon_0}{\mu_0}\,\mathbf{E}\times\mathbf{E}^*\,, \tag{1}$$

where a is the magneto-optical coefficient entering into the expression for the dielectric permittivity tensor of the material: $\varepsilon_{ij} = \varepsilon\delta_{ij} + \mathrm{i}a\epsilon_{ijk}M_k$, where δ_{ij} is the Kronecker symbol, ϵ_{ijk} is the Levi-Civita symbol, and M_k is the corresponding component of the magnetization vector of the medium. Expression (1) is derived on the basis of thermodynamic considerations for the nondissipative medium; however, the effective magnetic Faraday field also appears in the quantum-mechanical consideration in the second-order perturbation theory in the field amplitude [24]. Notice that the strength of the magnetic field H_F can reach several teslas.

The experiment in Ref. [23] was carried out on a single-crystal film of thickness $L = 5$ μm of a rare-earth iron garnet with bismuth substitution, grown by the method of liquid-phase epitaxy on a substrate of gadolinium–gallium garnet with a crystallographic orientation (111). The composition of the film determined by the method of electron microprobe analysis was $(Bi_{0.9}Lu_{1.4}Tm_{0.4}Sm_{0.1})(Fe_{4.6}Ga_{0.4})O_{12}$. The saturation magnetization of the film was $4\pi M_s \approx 850$ G, and the constant of the cubic anisotropy was $K_1 = 4.0\times10^4$ erg cm^{-3}. The magnetization dynamics was excited by femtosecond laser pump pulses with a time duration $t = 200$ fs and a repetition rate of 80 MHz. The pump pulses, which have circular polarization, fell on the sample at an angle of 17°. The precession of magnetization in the external magnetic field was observed with the aid of linearly polarized probe pulses incident on the sample at an angle of 17° in the plane orthogonal to the plane of incidence of the pump pulses. The time delay between the pump and probe pulses varied from 0.3 to 2.5 ns. As a result of the oscillations of the magnetization, the projection of the magnetization onto the wave vector of the probe pulse changed, which was registered based on the change in the Faraday angle Ψ of the probe pulse. The pump and probe pulses, which had a central wavelength of 650 and 820 nm, respectively, were focused on the surface of the film onto spots about 7 μm in diameter. The intensity of the probe pulses was an order of magnitude less than the intensity of the pump pulses, which made it possible to ignore the influence of the first ones on the magnetization of the sample.

Further, the difference between the signals that appear under the action on the sample of pulses with left-hand and right-hand (σ^+ and σ^-) circular polarizations was measured. The external magnetic field was applied perpendicularly to the plane of the sample and the plane of incidence of the pump pulses (Fig. 1). The edge of the absorption zone of the iron

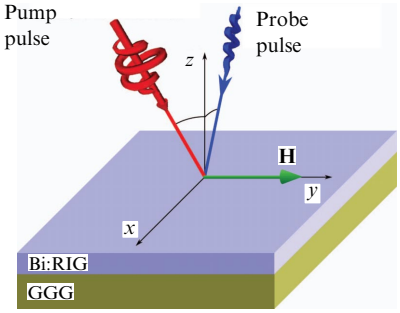

Figure 1. Diagram of experiment [23]. The surface of the sample lies in the plane xy. The external magnetic field is directed along the y-axis. The pump and probe pulses fall onto the sample in the mutually perpendicular planes yz and xz, respectively. Bi:RIG is a rare-earth iron garnet substituted with bismuth; GGG is the gadolinium–gallium garnet.

garnet is located in the region of $\lambda = 530$ nm; therefore, the transmission coefficient of the sample grows monotonically with an increase in the wavelength. The Faraday angle, on the contrary, diminishes with the growth of the wavelength: $\Psi_s = 3.1^\circ$ at $\lambda = 650$ nm (the wavelength of the pump pulse), and $\Psi_s = 1.3^\circ$ at $\lambda = 820$ nm (the wavelength of the probe pulse).

With the passage of the laser pulse, an effective magnetic field is induced in the magnetic sample, which is directed along the wave vector of the pump pulse. This field causes the magnetization to deviate from the equilibrium position and leads to a precession of the magnetization relative to its equilibrium position with a precession angle θ at a frequency $\omega = \gamma\sqrt{H(H + H_a)}$, where γ is the gyromagnetic ratio, and $H_a = 4\pi M_s - 2K_1/M_s$. Because of the dissipation, which is determined by the Gilbert damping constant α, the amplitude of the precession angle diminishes exponentially in the course of time: $\theta(t) = \theta_0 \exp(-t/\tau)\sin(\omega t)$, where θ_0 is the initial precession angle, and τ is the damping time. The precession leads to a change in the projection of the magnetization onto the wave vector $\mathbf{k}$ of the probe pulse, $M\theta$, where $\theta = \pi/2 - \theta_1$, and θ_1 is the angle between the magnetization and the vector $\mathbf{k}$. As a result, oscillations of the Faraday angle Ψ are observed (Fig. 2): $\Psi = \pi a M L\theta/(\lambda\sqrt{\varepsilon})$ (for $\theta \ll 1$) [14]. The observed signal is determined by the damped harmonic function: $\Psi = \Psi_0 \exp(-t/\tau)\sin(\omega t)$ with an amplitude $\Psi_0 = \pi a M L\theta_0/(\lambda\sqrt{\varepsilon})$. The approximation of the signal by the damped sine is shown by continuous black curves in Fig. 2. Using the Faraday angle Ψ_s, upon saturation of the magnetization of the film along the normal to the surface, we obtain $\Psi_0 = (M\theta_0/M_s)\,\Psi_s$.

On the other hand, the observed initial precession angle is determined by the value H_F of the IFE magnetic field averaged over the film thickness [23]:

$$\theta_0 = \gamma\sqrt{1 + \frac{H_a}{H}}\,\langle H_F\rangle\,\Delta t\,. \tag{2}$$

According to expression (1), for circularly polarized light one finds $\langle H_F\rangle = a\langle|E|^2\rangle$, where $\langle|E|^2\rangle$ is the square of the amplitude of the electric field strength in the film averaged over the film thickness, which is proportional to the field amplitude E_0 of the incident radiation with a coefficient $\sqrt{\kappa}$. The coefficient κ is determined from the Fresnel formula for the film. Taking into account equations (1), (2) and the expression $J = c\varepsilon_0 E_0^2 \Delta t/2$ for the surface density of the energy of the incident radiation, we obtain

$$\Psi_0 = 2\,\frac{a\gamma}{c\mu_0 M_s}\,\Psi_s M\kappa\sqrt{1 + \frac{H_a}{H}}\,J\,. \tag{3}$$

In this case, we assume that $M = M_s$. Thus, the amplitude of the observed signal is directly proportional to the energy density of the incident radiation.

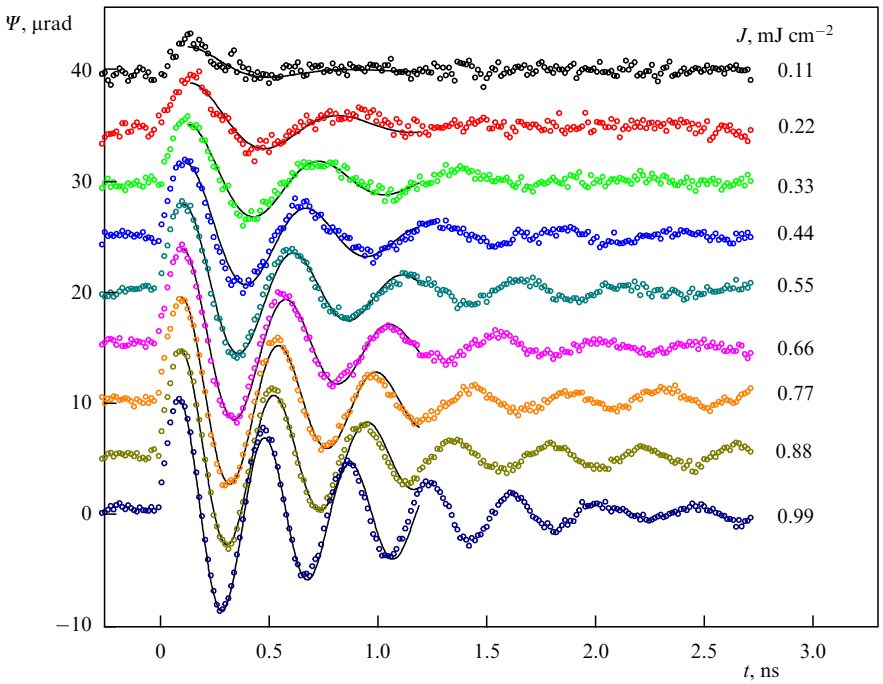

Figure 2. Precession of magnetization upon excitation by pump pulses with the wavelength $\lambda = 650$ nm and the energy density J from 0.11 to 0.99 mJ cm^{-2}. The external magnetic field $H = 89$ mT. The pump pulse acts on the sample at the moment of time $t = 0$ [23].

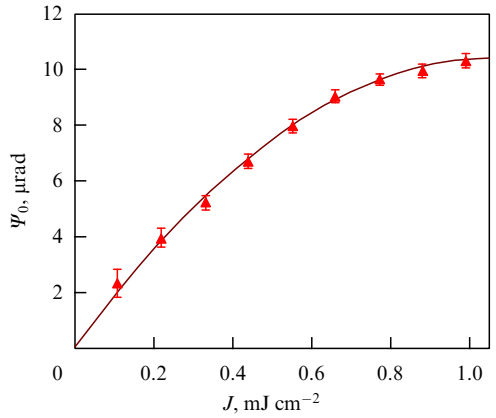

Figure 3. Experimental (triangles) and theoretical (solid curve) dependences of the Faraday effect on the energy density of pumping [23]. External magnetic field $H = 89$ mT. The best approximation of the experimental data is achieved at $b = 3300$ A mJ^{-1}.

The observed deviation of the experimental data from the linear law is connected with the generation of magnetostatic spin waves (MSWs). Indeed, when deriving equation (1), it was assumed that the excited precession of the magnetization was uniform in space. At the same time, upon excitation of the IFE in magnetically ordered materials by focused femtosecond pulses, the optical radiation acts directly only on the magnetization in the region of focusing the pumping beam (~ 7 μm) and then, mainly as a result of magnetic dipole–dipole interaction, magnetization oscillations appear in the adjacent regions and MSWs are excited [3, 25]. The MSWs remove part of the energy and, furthermore, lead to a nonuniform distribution of the magnetization in space. As a result, magnetization M, which enters into the expression for the observed Faraday angle (3), differs from the saturation magnetization $M = M_s - \delta M$ (where δM is the magnetization of the MSW averaged over the spot of the probe beam) and depends on the value of the IFE effective magnetic field and, consequently, on the energy of the incident radiation.

Expanding the dependence $\delta M(J)$ into a series in powers of J up to the first-order terms, we obtain a more precise expression for the dependence of the Faraday angle on the pump energy:

$$\Psi_0 = \frac{2a\gamma}{c\mu_0}\,\Psi_s\kappa\sqrt{1+\frac{H_a}{H}}\left(J - \frac{b}{M_s}\,J^2\right), \qquad (4)$$

where the parameter b can be found from experiment. Experimental and calculated results for the dependence of the Faraday angle on the pump energy density are given in Fig. 3.

Thus, it has been shown that the magnitude of the inverse Faraday effect depends on the density of the pump energy nonlinearly. This is explained by the excitation of MSWs, as a result of which the average value of the magnetization participating in the precession changes.

3. Dynamics of magnetization in thulium orthoferrite and photoinduced magnetic anisotropy

Another system in which the excitation of the ultrafast dynamics of magnetization with the aid of femtosecond laser pulses was studied is the ferromagnet $TmFeO_3$, which has a perovskite-like cell. It is assumed that the interaction of electromagnetic pulses with the magnetic medium has a magnetodipole character in combination with the spin–orbit coupling. In thulium orthoferrite, the ground state $^3H_6$ of the Tm^{3+} ion is split into a sequence of singlet levels with a characteristic energy splitting on the order of 1–10 meV [26]. Owing to the exchange and magnetodipole interactions, the angular momenta of these states are connected with the spins of iron ions Fe^{3+}. The electric field of an ultrashort laser pulse changes the orbital state of the electrons belonging to thulium ions, which affects the spin subsystem and leads to the appearance of a photoinduced magnetic anisotropy. Upon a sharp change in the magnetic anisotropy, in turn, a precession of magnetization begins.

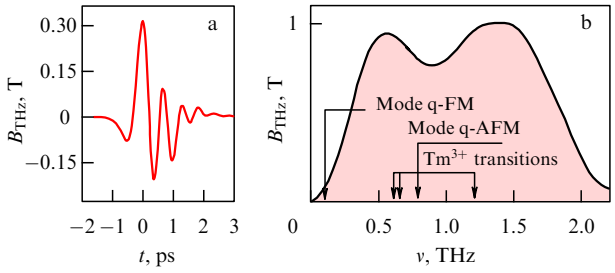

Figure 4. (a) Electro-optically measured time profile, and (b) the amplitude spectrum of the terahertz laser pump pulse, which was used in the experiment [27].

Two modes are present in the spin dynamics of an antiferromagnet: quasiferromagnetic (q-FM), and quasi-antiferromagnetic (q-AFM) ones. In experiments, the excitation of both modes was observed; the magnetic field strength of a terahertz laser pulse varied between 0.02 and 0.30 T, with the profile of the field remaining constant (Fig. 4). The measurements were conducted in the phase Γ_{24}, in which the antiferromagnetic vector $\mathbf{G}$ makes an angle $0 < \theta_0 < \pi/2$ with the plane (001) and with the [100]-axis in the quasi-cubic coordinate system. Figure 5 shows the amplitude of these two modes of oscillations depending on the magnetic field B_{THz} of the terahertz pulse.

Thus, it was experimentally found that the excitation of nonlinear spin dynamics occurs through the rare-earth subsystem, which creates an efficient spin torque acting on the spin subsystem of the Fe^{3+} ions [27]. For a theoretical description of the dynamics of the quasiferromagnetic mode, we will invoke the model of a weak ferromagnet relying on the Lagrange L and Rayleigh R functions of the following form [28]:

$$L = \frac{M_{Fe}}{2\gamma^2 H_E}\,\dot\theta^2 - \frac{M_{Fe}}{\gamma H_E}\,B_y\dot\theta - W(\theta), \qquad (5)$$

$$R = \frac{\alpha M_{Fe}}{2\gamma}\,\dot\theta^2. \qquad (6)$$

Here, M_{Fe} is the magnetization of the iron sublattice, H_E is the effective d–d exchange field, γ is the gyromagnetic ratio, α is the Gilbert damping constant, $\mathbf{B}$ is the magnetic field vector of the terahertz laser pulse, the angle θ parametrizes the antiferromagnetic vector $\mathbf{G} = (\cos\theta, 0, \sin\theta)$, and $W(\theta)$ is the free energy of the system, which can be represented in the

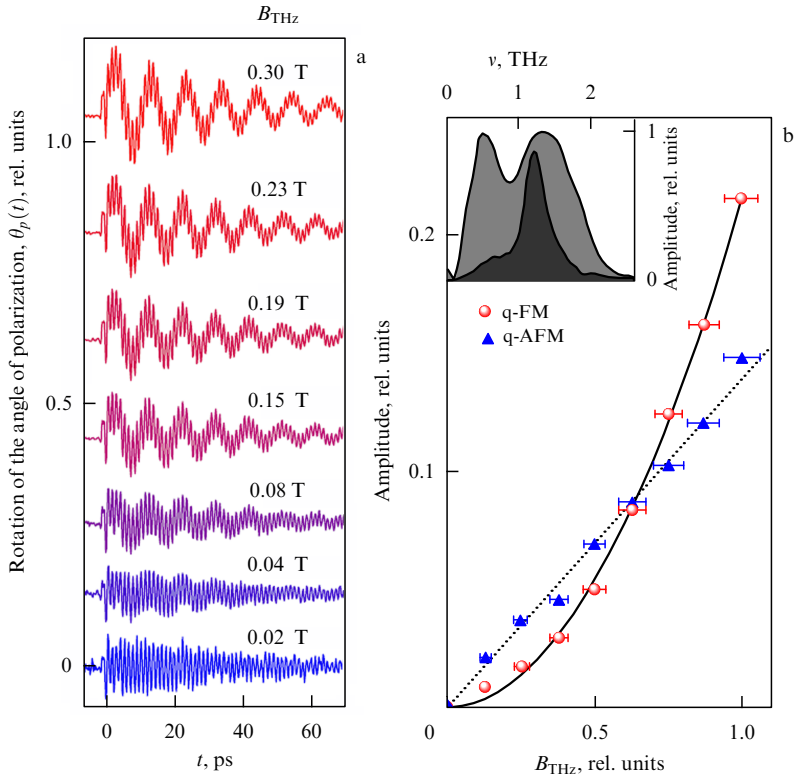

Figure 5. (a) Magneto-optical signal after excitation of a $TmFeO_3$ crystal by terahertz laser pump pulses with the intensity of the pulse magnetic field varying in the range of 0.02–0.30 T. (b) Dependence of the amplitude of the fluctuations of quasiferromagnetic and quasiantiferromagnetic modes on the magnetic field of the terahertz pump pulse upon application of a band-pass filter with a central frequency of 1.2 THz [see inset to figure (b)] [27].

following form:

$$W(\theta) = K_1 \sin^2\theta + K_2 \sin^4\theta + W_{ME} - \frac{H_D}{H_E} M_{Fe}(B_z \cos\theta - B_x \sin\theta)\,, \quad (7)$$

where K_1, K_2 are the constants of magnetic cubic anisotropy, H_D is the Dzyaloshinskii field, and the magnetoelectric term W_{ME} after the substitution into the equations of the dynamics corresponds to the optical spin torque, which describes the action of the laser pulse on the magnetic system. The magnetoelectric tensor g_{iklm}, through which the photomagnetic part of the free energy is expressed, can be constructed from the considerations of symmetry for the point group D_{2h}^{16}:

$$W_{ME} = \sum_{i,k,l,m} g_{iklm} G_l G_m E_i E_k$$
$$= \cos^2\theta(g_{11}E_x^2 + g_{12}E_y^2 + g_{13}E_z^2)$$
$$+ \sin^2\theta(g_{12}E_x^2 + g_{22}E_y^2 + g_{33}E_z^2) + \frac{1}{2} g_5 \sin(2\theta)\, E_x E_z\,, \quad (8)$$

where g_{ij} are the components of the tensor g_{iklm} in the Voigt notation. After simplification of the functional dependence of this energy, we obtain

$$W_{ME} = (\chi_y E_y^2 + \chi_z E_z^2)\sin^2\theta\,, \quad (9)$$

which can be considered an additive to the anisotropy energy $\Delta K_1 = \chi_y E_y^2 + \chi_z E_z^2$, where $\chi_y = g_{22} - g_{11}$, $\chi_z = g_{33} - g_{13}$.

To find the dynamics of magnetization, let us write down the Euler–Lagrange equation:

$$\frac{d}{dt}\frac{\partial L}{\partial \dot\theta} - \frac{\partial L}{\partial \theta} + \frac{\partial R}{\partial \dot\theta} = 0\,. \quad (10)$$

From this we find the equation of dynamics for the angle $\theta(t)$, which has the form of the generalized sine-Gordon equation:

$$\ddot\theta + \omega_E \alpha \dot\theta + 2\omega_E \omega_A \sin\theta\cos\theta(K_1 + K_2\sin^2\theta)$$
$$= \gamma \dot B_y - \frac{H_D}{H_E}\omega_E \gamma(B_z \sin\theta + \gamma B_x \cos\theta)$$
$$- \omega_E \omega_A \sin\theta\cos\theta\, a(t)\,, \quad (11)$$

where $a(t) = 2\Delta K/K_1$, $\omega_E = \gamma H_E$, and $\omega_A = \gamma K_1/(2M_{Fe})$.

For numerical calculations, the following set of parameters was used: $M_{Fe} = 1000$ CGS units cm^{-3}, $H_E = 2\times10^7$ Oe, $H_D = 2\times10^5$ Oe, and $\omega_E\alpha = 0.05$ ps^{-1}. Figure 6 shows the time evolution of the angle $\theta(t)$ without taking into account the additional photomagnetic anisotropy.

Thus, the quasiantiferromagnetic mode changes linearly with the growth of intensity, whereas the quasiferromagnetic mode manifests a nonlinear dependence, connected with the fact that the photomagnetic anisotropy playing an important role in the excitation of precession nonlinearly depends on the electric field of the pulse. In this case, the excitation of spins under the action of photomagnetic anisotropy is by a factor of eight stronger than the possible excitation caused by Zeeman interaction at the maximum magnetic field of the pulse, equal to 0.3 T [27].

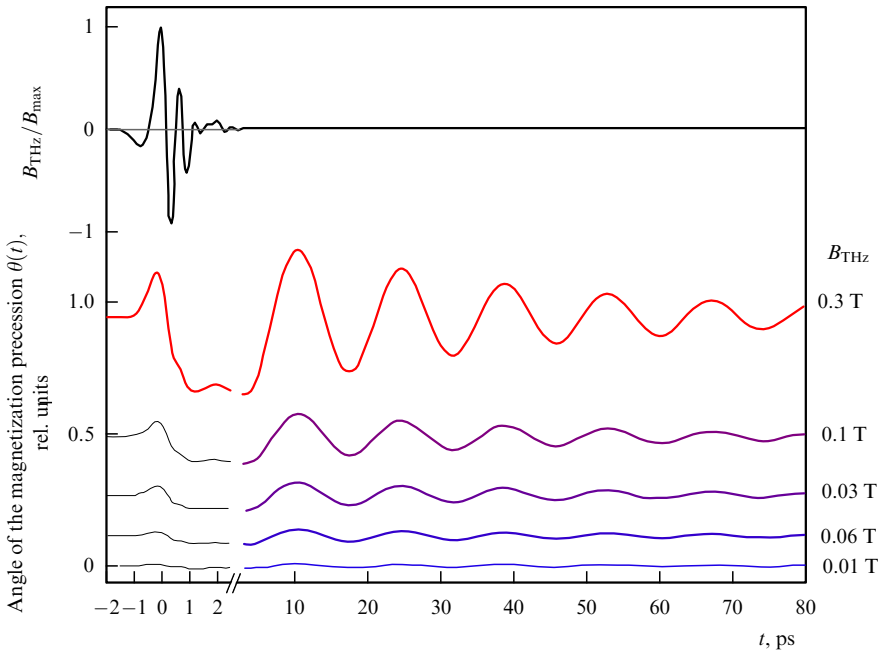

Figure 6. (Color online.) Theoretical calculation of the time dependence of magnetization precession described by the angle $\theta(t)$ for different peak amplitudes of the magnetic field of a laser pulse (shown by the black profile).

4. Dynamics of magnetization in the metallic ferrimagnet GdFeCo under the action of a demagnetizing femtosecond laser pulse

As the third example, let us consider the excitation of spin dynamics in thin ferrimagnetic GdFeCo films in the vicinity of the compensation point T_{comp}. At present, GdFeCo type ferrimagnets are used actively in spintronics, for example, in studies on recording information using femtosecond laser pulses [8, 16–19]. At temperatures lower than the compensation point, the magnetization of the d-sublattice is less than the magnetization of the f-sublattice; at temperatures higher than T_{comp}, it is vice versa. At the point of compensation, one has $|\mathbf{M}_d| = |\mathbf{M}_f|$. The properties of a material with a compensation point are close to the properties of antiferromagnets. They are characterized, in particular, by the presence of exchange type high-frequency spin waves and a weakened influence of magnetodipole interactions, which, as is known, determine the parasitic reciprocal influence involving the elements of the spintronics networks.

Ferrimagnetic materials possess interesting phase diagrams near the point of compensation [29–31]. Of special interest from the viewpoint of the processes of magnetization reversal of magnets by femtosecond laser pulses are spin-reorientation first-order transitions. It was shown that in the GdFeCo system there can be achieved a record low-energy consumption, on the order of 1 fJ, necessary for the recording of one bit with a characteristic recording–re-recording time equal approximately to 100 ps. The mechanism of the switching of a bit or, more generally, of the interaction of a femtosecond pulse with a ferrimagnetic material in the case of metals differ greatly from those examined above, and have so far been studied considerably less. This problem was first studied in pioneering paper [11], where a sharp decrease in the magnetization of nickel (demagnetization) was observed at the moment of the pulse action, with the subsequent gradual relaxation of the excitation on a time scale of less than 100 ps.

Let us examine how the demagnetization of a sample, i.e., a sharp decrease in the absolute value of the magnetization, can induce spin dynamics in GdFeCo. An amorphous GdFeCo film applied onto a substrate (for example, SiN) possesses a uniaxial magnetic anisotropy $K_1 \approx 5 \times 10^4$ J m^{-3}. In the presence of a magnetic field $\mathbf{H} \parallel \mathbf{n}$ ($\mathbf{n}$ is the normal to the film), we can move to a description of the system in terms of the antiferromagnetic vector $\mathbf{L}$, which is parametrized by a polar angle θ counted from the normal to the film and by an azimuthal angle φ. As a result, an effective Lagrangian of the form

$$\mathcal{L}_{eff} = m\cos\theta\left(H - \frac{\dot{\varphi}}{\gamma}\right) + \frac{\chi_\perp}{2}\sin^2\theta\left[\left(H - \frac{\dot{\varphi}}{\gamma}\right)^2 + \frac{2K_1}{\chi}\sin^2\varphi\right] + \frac{\chi_\perp}{2}\left(\frac{\dot{\theta}}{\gamma}\right)^2 \quad (12)$$

was obtained near the compensation point, where $m = M_d - M_f$, M_d and M_f are the magnetizations of the d- and f-sublattices, respectively, and $\chi_\perp$ is the transverse magnetic susceptibility.

The system under consideration has an axial symmetry; therefore, under the action of a femtosecond pulse with $\mathbf{k} \parallel \mathbf{n}$, the projection of the angular momentum $\mathcal{J} = -\partial\mathcal{L}_{eff}/\partial\dot{\phi}$ onto the normal to the film should be conserved. This projection contains two contributions:

$$\mathcal{J} = \frac{m}{\gamma}\cos\theta + \frac{\chi_\perp}{\gamma}\left(H - \frac{\dot{\varphi}}{\gamma}\right)\sin^2\theta\,. \quad (13)$$

The first contribution to the value of the angular momentum (13) is caused by the projection of the magnetization onto the normal to the film. The second contribution appears due to the anisotropic energy of the magnetization of the ferrimagnet by the effective field $H - \dot{\varphi}/\gamma$. Upon changing the magnetization by Δm, the second contribution, in view of the conservation of the angular momentum,

changes by a value ($t < 0$: $\dot{\varphi} = 0$)

$$\delta\left(H - \frac{\dot{\varphi}}{\gamma}\right) = -\frac{\Delta m}{\chi_\perp}\frac{\cos\theta_0}{\sin^2\theta_0}, \qquad (14)$$

where $0 < \theta_0 < \pi$ is the polar angle characterizing the canted phase, which arises at a certain constant external magnetic field H. A sharp change in the magnitude of $\dot{\varphi}$ caused by the pulse $\delta m(t)$ creates a spin torque T, which leads to a deviation of the polar angle θ from the equilibrium position. According to calculations, the magnitude of $\dot{\theta}(0)$ arising under the effect of the pulse $\delta m(t)$ has the following form:

$$\dot{\theta}(0) \approx \left[-\left(2\frac{\cos^2\theta_0}{\sin\theta_0} + \sin\theta_0\right)H + \frac{m_0}{\chi_\perp}\frac{\cos\theta_0}{\sin\theta_0} + \frac{2}{3}\frac{\Delta m}{\chi_\perp}\frac{\cos\theta_0}{\sin^3\theta_0}\right]\frac{\gamma^2}{\chi_\perp}\frac{1}{2}\Delta m\Delta t, \qquad (15)$$

where Δm is the total change in the magnetization under the action of the laser pulse, and Δt is the characteristic time of the demagnetization. An important consequence of equation (15) is the fact that the initial amplitude $\dot{\theta}(0)$ depends in a critical manner on the order parameter in the noncollinear phase of the ferrimagnet ($\sin\theta_0$). Thus, the effect of the excitation of the dynamics of magnetization by a demagnetizing femtosecond laser pulse should manifest itself especially strongly in the vicinity of phase transitions into the collinear phases, where $\theta_0 = 0, \pi$. Figure 7 plots the theoretical dependences of amplitude (15) on the field strength. At a temperature below the point of the phase transition, the system resides in the collinear phase, and the demagnetizing pulse causes no precession. At a field corresponding to the point of the second-order phase transition into the canted phase, a sharp increase in the amplitude is observed, which then decreases with growing field. A similar behavior was also observed in experiment [32] (Figs 7b, c).

Notice a certain analogy between the phenomenon under consideration and the Einstein–de Haas effect, in which the changing magnetic moment passes into the torque of the sample, whereas in our case (14) it is transferred into the precession moment of the magnetic subsystem described by the angle $\dot{\varphi}(t)$.

5. Spin pumping and inverse spin Hall effect

In Sections 2–4 we considered cases where the spin dynamics are detected with the aid of magneto-optical effects. However, of great interest for modern applications in the field of spintronics is another approach based on the electric detection of the magnetization dynamics. This method can be based on spin-orbit effects, for example, on the inverse spin Hall effect [33]. Below, we will examine the case in which the dynamics of magnetization in the nanostructure is excited by a microwave field acting on the sample. Among the promising materials in which these effects can be realized, it is worthwhile to note metals with large spin-orbit interaction (Pt, Au), as well as two-dimensional (2D) and three-dimensional (3D) topological insulators (Bi_2Se_3, Bi_2Te_2Se, etc.). Recently, a record-breaking high value of the factor of the charge-to-spin conversion was revealed in the 3D topological insulator Bi_2Se_3 [34]. In combination with the possibility of utilizing uncommon surface states, this makes 3D topological insulators especially attractive for creating spin-orbitronics devices [20, 21].

In recent years, numerous experimental studies have been devoted to spin injection in structures that can be

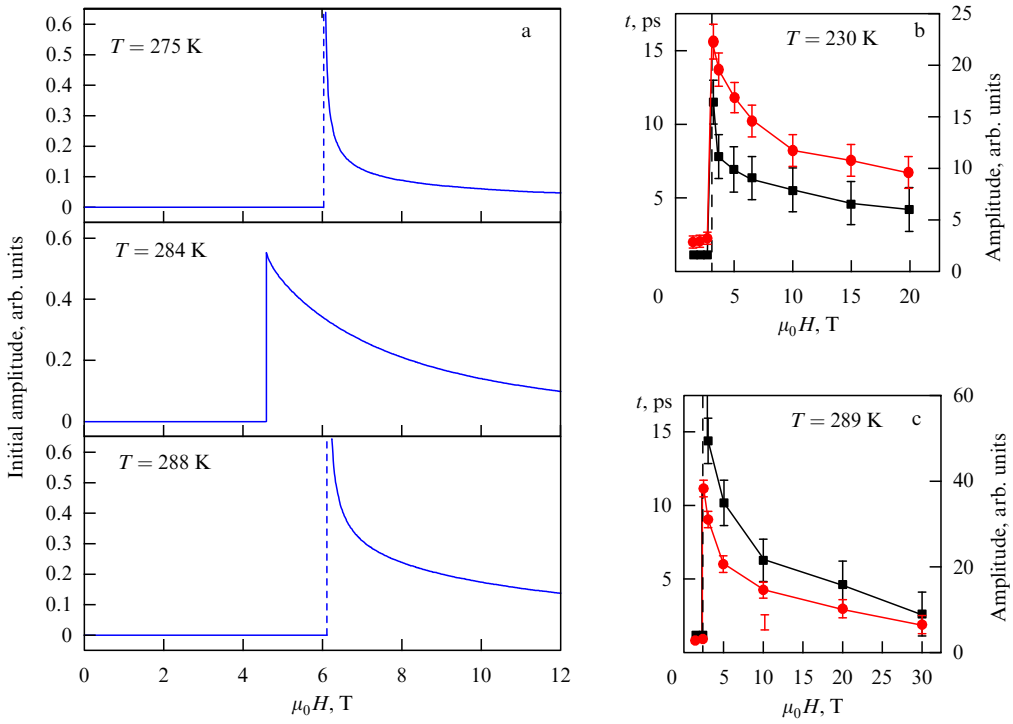

Figure 7. (a) Theoretical calculation of the initial amplitude of the magnetization oscillations in a GdFeCo film at temperatures below and higher than the compensation point ($T_{comp} = 283$ K), depending on the value of the external magnetic field; (b, c) measured values of the initial amplitude of the magnetization oscillations in a GdFeCo film (24% Gd, 66.5% Fe, 9.5% Co) and of the decay time depending on the value of the external magnetic field at temperatures of 230 and 289 K, respectively [32]. Experimental data are reproduced with permission from the authors of Ref. [32].

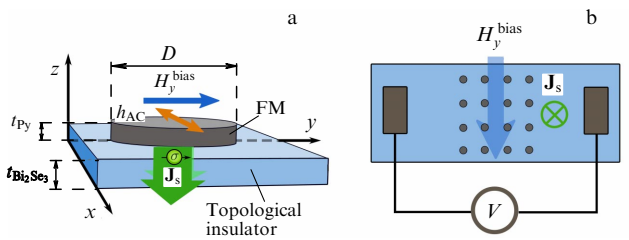

Figure 8. (a) Illustration of the principle of the experiment on spin pumping. A magnetostatic field H_y^{bias} and an AC magnetic field h_{AC} are applied to a ferromagnetic (FM) nanodot with a diameter D located on the surface of a topological insulator; as a result of the precession of magnetization, a spin current $\mathbf{J}_s$ is generated in the system. (b) Schematic of the measuring circuit of the voltage caused by the inverse spin Hall effect in a system consisting of a large number of nanodots located on the surface of a topological insulator.

described as 'ferromagnet/material with a giant spin-orbit interaction'. In these studies, the potential to efficiently generate a DC voltage as a result of the dynamics of magnetization excited in a ferromagnetic layer was shown [35, 36]. In such experiments, the magnetization dynamics is excited by a microwave field in a setup for measuring the ferromagnetic resonance, in the process of which a spin current flowing in the direction of the substrate is generated at the interface of the media between the ferromagnet and substrate (Fig. 8). In the substrate, where a giant spin-orbit interaction takes place, a conversion of the spin current into a charge current occurs (spin-to-charge conversion). The mechanism of this conversion may be the inverse Rashba–Edelstein effect [37], if the surface of the substrate possesses a substantial conductivity, or the inverse spin Hall effect [33], which appears with the flow of a spin current in the bulk of the substrate. Both these effects by their nature are directly caused by a spin-orbit interaction. As a result, the measurement of a constant voltage connected with the arising charge current is possible and has been carried out in practice [36, 38].

The spin pumping in heterostructures with a nonmagnetic metallic substrate is well described by the adiabatic microscopic theory (see, e.g., review [35]). There are also other, more general approaches, which can be applied to describing the spin pumping in a broad class of systems, for example, with a substrate made of a topological insulator [39]. Let us examine one of them. This approach is based on the reciprocity principle and on the known action of a spin-polarized current flowing through the system on the local magnetization in a ferromagnet [40]. Let us write down the generalized Landau–Lifshitz–Gilbert equation [40]

$$\dot{\mathbf{M}} = -\gamma \mathbf{M} \times \mathbf{H}_{\text{eff}} + \mathbf{T} + \frac{\alpha}{M_s} \mathbf{M} \times \dot{\mathbf{M}}\,, \tag{16}$$

where $\mathbf{H}_{\text{eff}}$ is the effective field acting on the magnetization, which is the sum of an external magnetic field and magnetostatic, exchange and anisotropy fields, α is the Gilbert damping constant, and $\mathbf{T}$ is the effective spin torque connected with the interaction between the spin-polarized current and the lattice spins. Assuming that $|\mathbf{M}| = \text{const}$ and that the current flows in the direction perpendicular to the layers, it is possible to resolve the effective spin torque into two perpendicular components along the vectors $\mathbf{M} \times \mathbf{j}_s$ and $\mathbf{M} \times \mathbf{M} \times \mathbf{j}_s$ ($\mathbf{j}_s$ is the vector whose value is proportional to the strength of the spin current and whose direction corresponds to its polarization):

$$\mathbf{T}_{\parallel} = -\frac{\gamma a_J}{M_s} \mathbf{M} \times \mathbf{M} \times \mathbf{j}_s\,, \tag{17}$$

$$\mathbf{T}_{\perp} = -\gamma b_J \mathbf{M} \times \mathbf{j}_s\,, \tag{18}$$

where a_J and b_J are the coefficients proportional to the current density, which depend on the parameters of the materials in the structure and on the characteristics of the interface. The first component of the spin torque is called adiabatic (the corresponding coefficient a_J can be obtained from experimental data or can be calculated from microscopics), and the second component is called nonadiabatic. In real systems, one usually finds $|b_J| \ll |a_J|$ [41].

Thus, if the value and the polarization of the spin current that is passed through a heterostructure with a magnetic material are known, it is possible to take into account its influence on the magnetization dynamics in the layer (to find $\dot{\mathbf{M}}$). In this case, the passage of the current through the magnetic layer exerts, in turn, an effect on its polarization as a consequence of exchange interaction and of the spin conservation law [42, 43]. The setting of the inverse problem is also possible: let the magnetization dynamics take place in a similar heterostructure; it is necessary to calculate the spin current generated in such a system. Indeed, resolving the vector $\mathbf{j}_s$ into three vectors, $\mathbf{M}$, $\mathbf{M} \times \dot{\mathbf{M}}$, $\mathbf{M} \times \mathbf{M} \times \dot{\mathbf{M}}$, and solving the inverse problem, disregarding the nonadiabatic term, we obtain

$$\mathbf{j}_s = \frac{1}{M_s^2} \frac{\hbar}{4\pi} g_{\text{eff}} \mathbf{M} \times \dot{\mathbf{M}}\,, \tag{19}$$

where g_{eff} corresponds to the spin-mixing constant, when a nonmagnetic metal is used as the substrate [35].

Upon substituting expression (19) into the spin torque in (16), we learn that the generation of a spin current in the adiabatic case leads to a change in the damping constant (this phenomenon is also called enhanced Gilbert damping [44]), which is usually determined from experiment. Let us introduce an effective damping constant $\alpha_{\text{eff}} = \alpha + \delta\alpha_{\text{sp}}$, where the second term is due to the departure of the magnetic moment in connection with the generation of a spin current at the interface between the magnetic layer and the substrate. This term is defined by the expression [35]

$$\delta\alpha_{\text{sp}} = g^{\text{eff}} \frac{g\mu_B}{4\pi M_s t_{\text{FM}}}\,, \tag{20}$$

where t_{FM} is the thickness of the ferromagnetic layer.

An important step on the way to applying the effect of spin pumping in real spintronics devices, such as MRAM (Magnetoresistive Random Access Memory) [45], spin diodes [46], and spin-transfer nano-oscillators [47], is the miniaturization of the structure. In connection with this, studies on the spin pumping effect in structurized materials are necessary. Measurements of the constant voltage which arises as a result of spin pumping in heterostructures consisting of Permalloy nanodots with a diameter of 200 nm (P_{200}/BS) and 400 nm (P_{400}/BS) applied onto the surface of the topological insulator Bi_2Se_3 (BS) have recently been carried out [38]. Two peaks were discovered in the signal of the DC voltage, which correspond to two different modes of the magnetization precession in nanodots (Fig. 9).

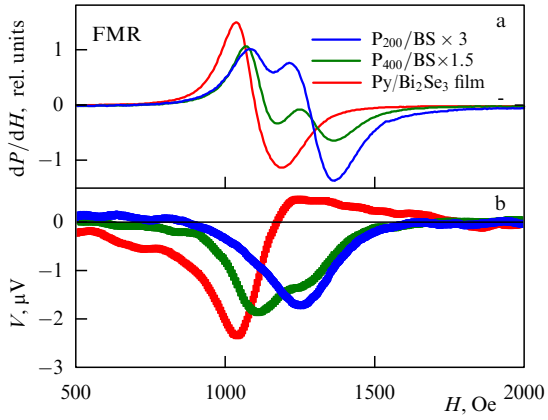

Figure 9. (a) Signal of the ferromagnetic resonance (FMR) from the P_{200}/BS (with the factor 3) and P_{400}/BS (with the factor 1.5) samples, and also the reference measurements for the bilayer Permalloy (Py)/Bi_2Se_3 structure. (b) DC voltage measured using the same samples in the experiment [38].

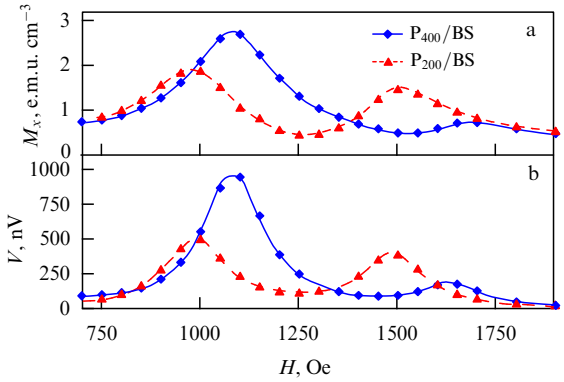

Figure 10. (a) Dependence of the x-component of magnetization (averaged over the period of oscillations and over the volume of the nanodot) on a DC component of the applied magnetic field (micromagnetic simulation). (b) Results of the numerical calculation of the dependence of the DC voltage generated in the P_{400}/BS samples and P_{200}/BS on the DC component of the applied magnetic field under the conditions of the experiment on spin pumping.

To simulate spin pumping in such systems with the aid of the program package SpinPM that we have developed, a micromagnetic simulation of the dynamics of magnetization in a nanodot was carried out taking into account the dissipation connected with the presence of a topological insulator as the substrate. In this case, the numerical integration of the Landau–Lifshitz equation was carried out with the adapted time step with the partition of the nanodot into cells with the dimensions of $2.5 \times 2.5 \times 10$ nm^3, taking into account the exchange interaction between the cells. The simulation was carried out under the conditions of ferromagnetic resonance, similar to the experimental conditions, when an AC magnetic field with a frequency of 9.8 GHz and amplitude of 0.44 Oe is directed along the x-axis (see Fig. 8), and a magnetostatic field, whose strength varies in the range of 500–2500 Oe, is applied along the y-axis. The following magnetic parameters of Permalloy were used: $M_s = 800$ CGS unit cm^{-1}; the constant of the exchange interaction $A = 1.3 \times 10^{-6}$ erg cm^{-1}; the effective Gilbert damping constant was selected in accordance with the experimental data, taking into account the enhancement of damping connected with the spin pumping effect; and $\alpha_{\text{eff}} = 0.0237$ and 0.0223 for samples with Permalloy nanodots with diameters of 200 and 400 nm, respectively.

Figure 10a displays the dependence of the x-component of the magnetization averaged over oscillation period and over nanodot for nanodots with diameters of 200 and 400 nm. It has been established that the low-field peak corresponds to a uniform (Kittel) mode of oscillations, and the high-field peak to a nonuniform, or magnetostatic, mode.

The spin current generated at the interface between the magnetic material and the substrate made of a topological insulator further flows in the volume of the topological insulator under the condition that its bulk conductivity be sufficiently high [48]. In the presence of a strong spin-orbit interaction, this leads to the flow of a charge current [33] according to the expression

$$(j_c)_i = \theta_{\text{ISHE}} \frac{2e}{\hbar} \epsilon_{ijk} n_j (j_s)_k , \qquad (21)$$

where **n** is the unit vector in the direction of the current flow, and the coefficient θ_{ISHE}, called the angle of the inverse spin Hall effect, for the topological insulator Bi_2Se_3 used in the experiment can take giant values, up to a record-high value of 0.38, recently found experimentally [34]. Figure 10b presents the results of the calculation of the ISHE DC voltage based on the micromagnetic simulation of the dynamics of magnetization and on expressions (19) and (21). The calculation of the voltage was performed for the samples with a geometry similar to that of the experimental samples: P_{200}/BS and P_{400}/BS with the size of 0.5×1.0 mm with Permalloy nanodots with a thickness of 4 nm deposited in the form of a square lattice with a period of 1 μm. It can be seen from the results of simulations that both these modes of the magnetization precession, uniform and nonuniform, are quite efficiently converted into voltage.

6. Conclusions

Thus, three key examples of the mechanisms of excitation of ultrafast spin dynamics in magnets under the action of femtosecond laser pulses have been considered in this article. The study of the ultrafast dynamics of magnetization in transparent iron-garnet films, in which the excitation of the precession of magnetization is connected with the inverse Faraday effect, has shown the importance of taking into account magnetostatic spin waves in the practical problems of ultrafast magnetism. In the case of iron-garnet film, the influence of magnetostatic spin waves leads to a nonlinear dependence of the magnitude of the inverse Faraday effect on the pump power. Another mechanism is connected with the appearance of a photoinduced magnetic anisotropy, which was considered based on the example of thulium orthoferrite. In addition, it has been shown that the amplitude of the quasiferromagnetic mode of spin precession, in contrast to the amplitude of the quasiantiferromagnetic mode, manifests a nonlinear dependence on the magnetic field of the pump pulse. The reason for this is the nonlinear dependence of the photomagnetic anisotropy and, as a consequence, of the spin torque, on the field of the electromagnetic pulse. The excitation of ultrafast dynamics is also possible upon driving of the system from the equilibrium state due to the demagnetizing action of the laser pulse. A clear example of a material in which this mechanism occurs is GdFeCo — a promising

ferrimagnet for creating devices of magnetic storage and terahertz spintronics.

In heterostructures described as 'magnetic material/material with a strong spin-orbit interaction' with the excitation of the magnetization dynamics by a femtosecond laser pulse, spin pumping occurs. As a result of this the spin current flows from the magnetic layer into the substrate, and, as a result of the inverse spin Hall effect, is converted into a charge current, which can easily be detected. As an important example, the process of spin pumping has been considered in a system with a structured magnetic material, represented in the form of nanodots, in which a topological insulator Bi_2Se_3 is used as the nonmagnetic material possessing outstanding properties from the viewpoint of the strength of spin–orbit interaction and the spin-to-charge conversion factor. It has been established that the special features of the magnetization precession, such as the presence in it of two modes in the case of nanodots made of the NiFe ferromagnet, are transferred efficiently into the voltage, which is measured nonlocally.

Thus, the application of similar heterostructures in experiments on the excitation of the ultrafast dynamics of magnetization is of great interest both from the fundamental and practical viewpoints in the fields of spin-orbitronics, magnonics, and magnetic memory.

Acknowledgments

We are grateful to our co-authors, who permitted us to use in this article the experimental results from papers [23, 27, 38]. The work was supported by the Russian Science Foundation (project No. 17-12-01333).

References

1. Bossini D et al. *ACS Photon.* **3** 1385 (2016)
2. Kimel A V et al. *Nature* **435** 655 (2005)
3. Satoh T et al. *Nature Photon.* **6** 662 (2012)
4. Hansteen F et al. *Phys. Rev. B* **73** 014421 (2006)
5. Reid A H M et al. *Phys. Rev. Lett.* **105** 107402 (2010)
6. Mikhaylovskiy R V, Hendry E, Kruglyak V V *Phys. Rev. B* **86** 100405(R) (2012)
7. Reid A H M et al. *Phys. Rev. B* **81** 104404 (2010)
8. Stanciu C D et al. *Phys. Rev. Lett.* **99** 047601 (2007)
9. Deb M et al. *Appl. Phys. Lett.* **107** 252404 (2015)
10. Koopmans B et al. *Phys. Rev. Lett.* **85** 844 (2000)
11. Beaurepaire E et al. *Phys. Rev. Lett.* **76** 4250 (1996)
12. Atoneche F et al. *Phys. Rev. B* **81** 214440 (2010)
13. Stupakiewicz A et al. *Nature* **542** 71 (2017)
14. Zvezdin A K, Kotov V A *Magnitooptika Tonkikh Plenok* (Magneto-Optics of Thin Films) (Moscow: Nauka, 1988)
15. Belotelov V I, Zvezdin A K *Phys. Rev. B* **86** 155133 (2012)
16. Hohlfeld J et al. *Phys. Rev. B* **65** 012413 (2001)
17. Graves C E et al. *Nature Mater.* **12** 293 (2013)
18. Hashimoto Y et al. *Rev. Sci. Instrum.* **85** 063702 (2014)
19. Le Guyader L et al. *Appl. Phys. Lett.* **101** 022410 (2012)
20. Kuschel T, Reiss G *Nature Nanotechnol.* **10** 22 (2015)
21. Soumyanarayanan A et al. *Nature* **539** 509 (2016)
22. Walowski J, Münzenberg M *J. Appl. Phys.* **120** 140901 (2016)
23. Kozhaev M A et al. *JETP Lett.* **104** 833 (2016); *Pis'ma Zh. Eksp. Teor. Fiz.* **104** 851 (2016)
24. Pershan P S *Phys. Rev.* **130** 919 (1963)
25. Chernov A I et al. *Phys. Solid State* **58** 1128 (2016); *Fiz. Tverd. Tela* **58** 1093 (2016)
26. Srinivasan G, Slavin A N (Eds) *High Frequency Processes in Magnetic Materials* (Singapore: World Scientific, 1995)
27. Baierl S et al. *Nature Photon.* **10** 715 (2016)
28. Zvezdin A K et al. *JETP Lett.* **29** 553 (1979); *Pis'ma Zh. Eksp. Teor. Fiz.* **29** 605 (1979)
29. Goranskii B P, Zvezdin A K *Sov. Phys. JETP* **30** 299 (1970); *Zh. Eksp. Teor. Fiz.* **57** 547 (1969)
30. Zvezdin A K, Matveev V M *Sov. Phys. JETP* **35** 140 (1972); *Zh. Eksp. Teor. Fiz.* **62** 260 (1972)
31. Zvezdin A K *Handbook Magn. Mater.* **9** 405 (1995)
32. Becker J et al. *Phys. Rev. Lett.* **118** 117203 (2017)
33. Saitoh E et al. *Appl. Phys. Lett.* **88** 182509 (2006)
34. Mellnik A R et al. *Nature* **511** 449 (2014)
35. Tserkovnyak Ya et al. *Rev. Mod. Phys.* **77** 1375 (2005)
36. Baker A A et al. *Sci. Rep.* **5** 7907 (2015)
37. Edelstein V M *Solid State Commun.* **73** 233 (1990)
38. Han H C et al. *Appl. Phys. Lett.* **111** 182411 (2017)
39. Chen K, Zhang S *Phys. Rev. Lett.* **114** 126602 (2015)
40. Zvezdin A K, Zvezdin K A, Khval'kovskii A V *Phys. Usp.* **51** 412 (2008); *Usp. Fiz. Nauk* **178** 436 (2008)
41. Zimmler M et al. *Phys. Rev. B* **70** 184438 (2004)
42. Tatara G, Kohno H *Phys. Rev. Lett.* **92** 086601 (2004)
43. Ralph D, Stiles M *J. Magn. Magn. Mater.* **320** 1190 (2008)
44. Tserkovnyak Ya, Brataas A, Bauer G E W *Phys. Rev. Lett.* **88** 117601 (2002)
45. Tehrani S et al. *IEEE Trans. Magn.* **35** 2814 (1999)
46. Kiselev S I et al. *Nature* **425** 380 (2003)
47. Tulapurkar A A et al. *Nature* **438** 339 (2005)
48. Jamali M et al. *Nano Lett.* **15** 7126 (2015)